

Bayesian Approach to Find a Long-Term Trend in Erratic Polarization Variations Observed in Blazars

Makoto UEMURA¹, Koji S. KAWABATA¹, Mahito SASADA², Yuki IKEJIRI²,
Kiyoshi SAKIMOTO², Ryosuke ITOH², Masayuki YAMANAKA², Takashi OHSUGI¹,
Shuji SATO³, and Masaru KINO³

¹*Hiroshima Astrophysical Science Center, Hiroshima University, Kagamiyama 1-3-1,
Higashi-Hiroshima 739-8526
uemuram@hiroshima-u.ac.jp*

²*Department of Physical Science, Hiroshima University, Kagamiyama 1-3-1,
Higashi-Hiroshima 739-8526*

³*Department of Physics, Nagoya University, Furo-cho, Chikusa-ku, Nagoya 464-8602*

(Received 2009 October 9; accepted 2009 November 16)

Abstract

We developed a method to separate a long-term trend from observed temporal variations of polarization in blazars using a Bayesian approach. The temporal variation of the polarization vector is apparently erratic in most blazars, while several objects occasionally exhibited systematic variations, for example, an increase of the polarization degree associated with a flare of the total flux. We assume that the observed polarization vector is a superposition of distinct two components, a long-term trend and a short-term variation component responsible for short flares. Our Bayesian model estimates the long-term trend which satisfies the condition that the total flux correlates with the polarized flux of the short-term component. We demonstrate that assumed long-term polarization components are successfully separated by the Bayesian model for artificial data. We applied this method to photopolarimetric data of OJ 287, S5 0716+714, and S2 0109+224. Simple and systematic long-term trends were obtained in OJ 287 and S2 0109+224, while no such a trend was identified in S5 0716+714. We propose that the apparently erratic variations of polarization in OJ 287 and S2 0109+224 are due to the presence of the long-term polarization component. The behavior of polarization in S5 0716+714 during our observation period implies the presence of a number of polarization components having a quite short time-scale of variations.

Key words: galaxies: active — galaxies: nuclei

1. Introduction

Blazars are believed to be active galactic nuclei (AGN) with relativistic jets pointing toward us (e.g. Blandford & Rees 1978). Doppler-boosted non-thermal emission from the jet dominates from radio to γ -rays in blazars. The radio—optical emission is dominated by synchrotron emission, and hence, highly polarized. Polarimetric observations have been extensively performed since they provide a clue for the structure of magnetic field in the jet (e.g. Angel & Stockman 1980; Mead et al. 1990). Another important feature of blazars is a violent variability in a wide range of time-scales from a few minutes to years (e.g. Hufnagel & Bregman 1992). Since the polarization degree (PD) and angle (PA) are also variable with time, dense and long-term polarimetric observations are essential to understand the variation mechanism of blazars and the magnetic field structure in the jet.

Moore et al. (1982) conducted an intensive observation campaign for BL Lac with multi-longitude optical observatories over a week period, and found that the polarization changes trace out a random walk in the Stokes QU plane. In general, erratic variations have been observed in polarization of most blazars (e.g. Angel & Stockman 1980).

On the other hand, systematic variations in PD and PA were also occasionally detected in blazars, for example, flares associated with the increase of PD (Smith et al. 1986; Tosti et al. 1998; Efimov & Shakhovskoy 1998) and the color variation correlating with the variation in PD (Cellone et al. 2007). Marscher et al. (2008) have recently reported a smooth rotation of the polarization vector in BL Lac, which indicates a propagation of the emitting region through a helical magnetic field in the jet. Thus, both erratic and systematic variations of polarization have been observed in blazars.

The erratic variation of the polarization vector can be explained by a scenario that a number of independent sources with randomly oriented and strong polarizations blink (Moore et al. 1982; Impey et al. 1989; Jones et al. 1985). The systematic variations are, however, difficult to be explained only by the random variation. Alternatively, a number of systematic variations can be apparently overlooked in PD and PA if short-term polarization variations are superimposed on a long-term polarization trend. A schematic example is shown in figure 1. The upper and lower panels show the light curve of the total and polarized fluxes and the temporal variation of the polarization vector in the Stokes QU plane, respectively. In this example,

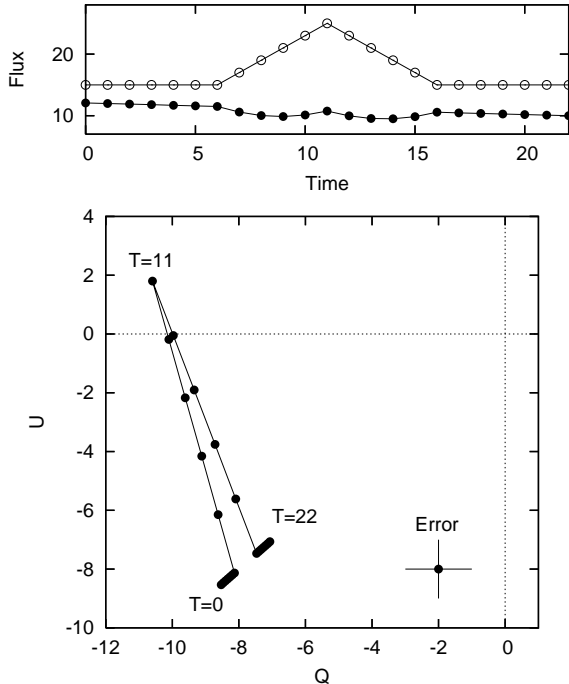


Fig. 1. Example of the short-term flare in the artificial data for our Bayesian model. The upper panel shows the light curve of the total and polarized fluxes indicated by the open and filled circles, respectively. The lower panel shows the temporal variation of polarization in the Stokes QU plane. A given error for the points is shown in the right-lower corner of the panel.

the polarization vector is assumed to be a superposition of two components; one shows a short-term variation associated with a flare of the total flux, and the other is a long-term trend. In the case that there is no long-term trend, PF correlates with the total flux, independent of the PA of the short-term flare. In the case that the long-term trend has a significant PF as shown in the lower panel of figure 1, however, the PF can show no positive correlation with the light curve. If the PA of the short-term flare is random and observations are sparse, the variation of polarization can be apparently erratic.

The presence of the long-term component has been suggested by several observations. The short-term variability of blazars is characterized by a combination of shots (Hufnagel & Bregman 1992). A typical time-scale of the shot was estimated to be ~ 1 d (Takahashi et al. 2000; Kataoka et al. 2001). In addition to these short-term variations, it is well known that blazars show variations with a time-scale of months–years. It is possible that the long- and short-term variation components have different polarization features. Marscher et al. (2002) reported VLBI radio observations of blazars, which show two or more components in polarization maps. If the polarization components in the radio range can be observed also in the optical range, an observed optical polarization vector should be a composition of those distinct radio polarization components since the angular resolution of optical observations

is much lower than that of VLBI radio images. Hagen-Thorn et al. (2002) reported a long polarimetric monitoring of BL Lac in 1969–1991, and found the existence of the preferred direction of the polarization vector. They propose a model that the polarization of BL Lac has two kinds of sources, a stationary component and a large number of randomly polarized components (also see, Blinov & Hagen-Thorn 2009). This stationary component could be considered as a long-term trend if it varies gradually.

The two-component model shown in figure 1 is one of the simplest one among models with multiple polarization components. It deserves further investigation if such a simple model can extract a systematic trend from erratic variations of polarization in blazars. Here, we present an exploratory Bayesian approach to separate a long-term trend from observed temporal variations of polarization in blazars. A description of the model and method is shown in the next section. We apply the model to observed photopolarimetric data of blazars and discuss the implications of the results in section 3. In section 4, we discuss the validity of the model and results. Finally, we summarize our findings in section 5.

2. Bayesian Model for the Separation of Long- and Short-Term Variation Components in Polarization

2.1. Model Description

We assume following three conditions for the observed flux and polarization in blazars. i) An observed polarization vector is a superposition of two distinct polarization vectors of long- and short-term variation components. ii) The short-term component is responsible for observed variations of the total flux. In other words, the PF of the short-term component completely correlates with the light curve of the total flux. iii) Temporal variations of the flux from the long-term component is small. Condition ii) is based on the fact that several flares of blazars are associated with the increase of PF, as mentioned in section 1. In our picture, all flares are associated with PF flares although each variation is often hidden in the observed PF because of the presence of the stronger, long-term component. Condition iii) is made just for simplicity of calculation. It is difficult to separate the short- and long-term components simultaneously in both the light curve and the polarization vector in our model.

Since Stokes parameters are additive, condition i) can be expressed with Stokes parameters Q and U as follows:

$$\begin{cases} Q_{\text{obs}} = Q_L + Q_S, \\ U_{\text{obs}} = U_L + U_S, \end{cases} \quad (1)$$

where $(Q_{\text{obs}}, U_{\text{obs}})$, (Q_L, U_L) , and (Q_S, U_S) denote the linear polarization parameters of the observed, long-, and short-term components, respectively. The short-term component (Q_S, U_S) is determined when (Q_L, U_L) is given for $(Q_{\text{obs}}, U_{\text{obs}})$. PF, PD and PA are calculated as $\sqrt{Q^2 + U^2}$, PF/I , and $\frac{1}{2} \arctan(U/Q)$, respectively.

Bayesian statistics provides a method to estimate a posterior probability density function (PDF) of model param-

eters from a likelihood function defined by the model and the data and a prior PDF of the model parameters. We develop a Bayesian model to estimate a time-series of Q and U of the long-term trend, that is, $\mathbf{y} = \{Q_{L,i}, U_{L,i}\}$ ($i = 0 - N$). We use N sets of photopolarimetric observations, $\mathbf{x} = \{Q_{\text{obs},i}, U_{\text{obs},i}, I_{\text{obs},i}\}$, where I_{obs} denotes the observed total flux. According to the Bayesian theorem, the posterior distribution of \mathbf{y} is calculated as:

$$P(\mathbf{y}|\mathbf{x}) = \frac{L(\mathbf{y}|\mathbf{x})\pi(\mathbf{y})}{C}, \quad (2)$$

where C is a constant for normalization of PDF. Here, $L(\mathbf{y}|\mathbf{x})$ and $\pi(\mathbf{y})$ are the likelihood function and the prior distribution of \mathbf{y} , respectively.

The likelihood function, $L(\mathbf{y}|\mathbf{x})$, is defined based on our assumed condition ii) and iii). The PF of the short-term component can be calculated as $\text{PF}_S = \sqrt{Q_S^2 + U_S^2}$. We normalized I_{obs} and PF_S using the, so-called, ‘‘Z-score’’ transformation defined as $a' = (a - \bar{a})/\sigma_a$, where a' , a , \bar{a} , and σ_a are the normalized and original parameter values, its average, and standard deviation, respectively. This normalization procedure reduces the uncertainty of a possible contribution of the long-term component to the total flux if the contribution is time-independent as assumed in condition iii). The likelihood function is, then, defined with these normalized parameters, I'_{obs} and PF'_S , as follows:

$$L(\mathbf{y}|\mathbf{x}) = \prod_i \frac{1}{\sqrt{2\pi\sigma_{\text{PF}'_i}^2}} \exp\left\{-\frac{(I'_{\text{obs},i} - \text{PF}'_{S,i})^2}{2\sigma_{\text{PF}'_i}^2}\right\}, \quad (3)$$

where $\sigma_{\text{PF}'_i}$ is the error for PF'_S . $\sigma_{\text{PF}'_i}$ is approximately given by the error of the observed PF. We neglected the error of I_{obs} because photometric errors of the total fluxes are much smaller than the errors of polarization parameters. $L(\mathbf{y}|\mathbf{x})$ reaches the maximum when the profile of the light curve is the same as that of PF_S .

The prior distribution, $\pi(\mathbf{y})$, plays a role in the control of the time-scale of the long-term trend in our model. Our model requires that the variation time-scale of (Q_L, U_L) is longer than that of (Q_S, U_S) . A long-term variation definitely draws a smoother path than that of short-term variations. A smooth curve can be described by a condition that a sequence of the first difference of $\{Q_{L,i}\}$ and $\{U_{L,i}\}$ follows a standard normal distribution. We define the prior distribution as follows;

$$\pi(\mathbf{y}) = \pi(\{Q_{L,i}\})\pi(\{U_{L,i}\}), \quad (4)$$

$$\pi(\{Q_{L,i}\}) = \prod_i \frac{1}{\sqrt{2\pi w^2}} \exp\left\{-\frac{(Q_{L,i} - Q_{L,i-1})^2}{2w^2}\right\}, \quad (5)$$

$$\pi(\{U_{L,i}\}) = \prod_i \frac{1}{\sqrt{2\pi w^2}} \exp\left\{-\frac{(U_{L,i} - U_{L,i-1})^2}{2w^2}\right\}. \quad (6)$$

$\pi(\mathbf{y})$ has no physical meaning in our model. It only controls the smoothness of the long-term trend by a hyperparameter, w . The result obtained with this model evidently depends on w . We determine an appropriate w using so-called ‘‘empirical Bayesian’’ approach, by making a criterion for obtained results, which are discussed in

subsection 2.3 and subsection 4.1. The hyperparameter, w , has the same dimension as Q and U . Since w corresponds to a standard deviation of a normal distribution as can be seen in equations (5) and (6), it is useful to use w normalized by a typical observation error of QU , σ ;

$$\sigma = \frac{\sum_{i=1}^N \sqrt{Q_{\text{err},i}^2 + U_{\text{err},i}^2}}{N}, \quad (7)$$

where $Q_{\text{err},i}$ and $U_{\text{err},i}$ are the observation error of $Q_{\text{obs},i}$ and $U_{\text{obs},i}$, respectively. In subsection 3.2, we discuss the dependence of the result on w/σ .

Thus, we can calculate $L(\mathbf{y}|\mathbf{x})$ and $\pi(\mathbf{y})$ for \mathbf{y} using the observations, \mathbf{x} . The posterior probability, $P(\mathbf{y}|\mathbf{x})$, was then estimated based on equation (2). The estimation was performed with the Markov Chain Monte Carlo (MCMC) method with the Metropolis algorithm (Metropolis 1953). The calculation procedure of MCMC is as follows: At the n -th step of MCMC, we obtain $p_n = L_n \pi_n$ for \mathbf{y}_n . We then randomly move to another point in the parameter space of \mathbf{y} by adding random values drawn from a standard normal distribution which has a dispersion chosen to efficiently sample the likelihood surface. As a result, we obtain p_{n+1} . We count the $(n+1)$ -th step if either $p_{n+1} > p_n$ or p_{n+1}/p_n is larger than a uniform random number between 0 and 1. Otherwise, we reject it and rework the $(n+1)$ -th step. After discarding the first 10^4 steps, we sample every 100 steps until the number of the sample becomes 10^5 . This procedure forms a set of \mathbf{y} , and we obtained ten sets of \mathbf{y} with different initial values of \mathbf{y} . We confirmed that no significant difference was seen in each set of \mathbf{y} . We merged them, and finally, obtained the MCMC sample of \mathbf{y} . The median and 68.3% confidence intervals for \mathbf{y} were determined from this combined sample.

2.2. Demonstration with Artificial Data

In this section, we demonstrate how our Bayesian model works using artificial data sets. We generated five sets of artificial data of temporal QU variations and light curves. Each data set consists of 100 sets of Q , U , and I in a time-series from $t = 0$ to 99. The duration and amplitude of the short-term flare were fixed in the light curve and PF as $\Delta t = 10$, $\Delta I = 10$, and $\Delta \text{PF}_S = 10$. Errors of Q and U were set to be 1.0. We used simple linear functions for brightening and fading phases of the flare. Figure 1 shows an example of the flare. Results of our analysis are independent of the flux out of the flare since the light curve is normalized in our procedure, as mentioned above. The short-term flares were randomly generated in the time and PA. The frequency of the flare was controlled with a parameter, α , which is a probability that a flare occurs at each time. Overlaps of flares were allowed. Figure 2 and 3 shows the variations in the QU plane and the light curves of the five sets of artificial data, labeled as (a), (b), (c), (d), and (e), respectively. We assumed sine-curves for the long-term trend, as depicted in the left panels of figure 2. The middle panels show $(Q_{\text{obs}}, U_{\text{obs}}) = (Q_L + Q_S, U_L + U_S)$.

We applied our Bayesian model to those artificial data. The hyperparameter, w , was fixed to $w/\sigma = 0.20$ in all

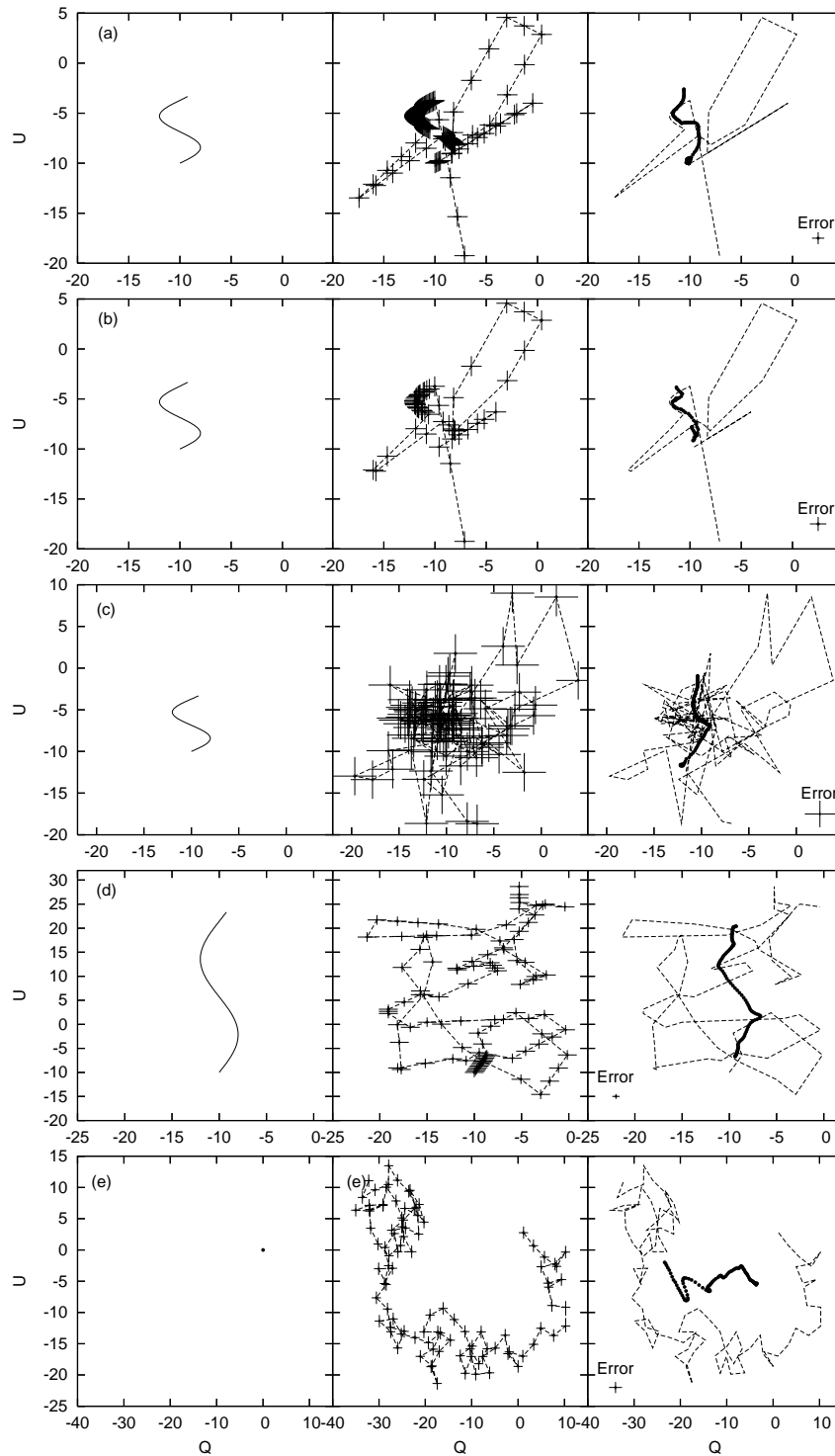


Fig. 2. Artificial polarization data and estimated long-term trends in the QU plane. Five sets of the data were used, as labeled (a), (b), (c), (d), and (e) (for the details of the data, see the text). The left, middle, and right panels show the assumed long-term trends, the short-term variations superimposed on the long-term trends, and the estimated long-term trends, respectively. The paths of the QU variation of the data are also shown in the right panels with the dashed lines. In Data (e), no long-term trend was assumed. The Bayesian estimations of the long-term trend were performed with $w/\sigma = 0.20$ in all cases.

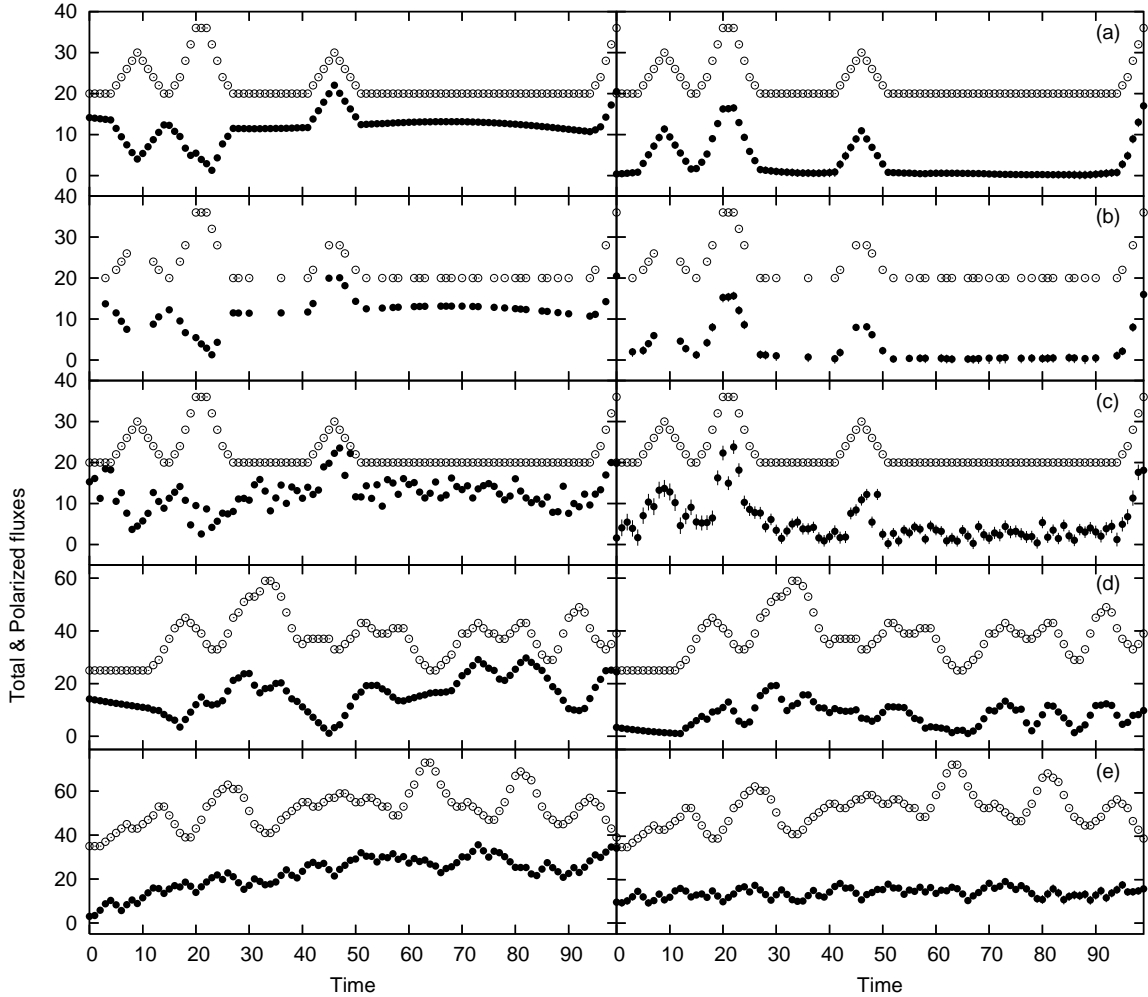


Fig. 3. Light curve of the total and polarized fluxes of the five sets of the artificial data labeled as (a), (b), (c), (d), and (e), indicated by the open and filled circles, respectively. In the right panels, the estimated long-term trends were subtracted from the polarized flux.

cases. The estimated long-term trends were shown in the right panels of figure 2, indicated by the filled circles. Typical errors of (Q_L, U_L) are also shown in each panel. The temporal variations of PF_S are shown in the right panels in figure 3.

Data (a) was generated with a low flare frequency of $\alpha = 0.02$. The second and fourth flares apparently have larger amplitudes than the others in the light curve because two consecutive flares are incidentally overlapped. A sign of the assumed long-term trend can be seen in the middle panel of figure 2 because of the low flare frequency. The observed PF apparently shows anti-correlations with the light curve in the flares of $t < 30$, while positive correlations are seen in $t > 30$. This is because the long-term trend has a significant polarization, and the polarization vectors of the early flares, incidentally, directed to the origin of the QU plane. As seen in figure 2, the Bayesian model well reproduced the assumed long-term trend. The corrected PF_S shows a clear correlation with the light curve in all period, as can be seen in figure 3.

Data (b) was generated from Data (a) by random sampling. We “observed” Data (a) with an observation probability of 50 %. This data is used in order to evaluate the Bayesian model for data taken with unequal time intervals, like typical ground-based observations of blazars. This experiment is important because the prior distribution in our model assumes data observed with equally-spaced intervals. The estimated PF_S still shows a clear correlation with the light curve. The estimated long-term trend is somewhat smoother than the assumed one, while it successfully reproduces general features of the assumed trend.

Data (c) is an example for data with a low signal-to-noise ratio (S/N). We generated Q and U of Data (c) by adding a Gaussian noise to those of Data (a) with standard deviations of Q and U of 2.3. This corresponds to $S/N = 3.0$ for each polarization flare having an amplitude of $\Delta PF_S = 10$. The estimated long-term component still shows a general trend of increasing U , while the “S”-shaped profile is weak. The correlation between

the light curve and PF is improved even in the case that this long-term trend is subtracted, as can be seen in figure 3. This is probably because the sub-structure of the assumed long-term trend is negligible compared with the flares having a large amplitude in this case. We confirmed that the estimation of the long-term trend was completely failed if the standard deviation of the Gaussian noise was 3.5 ($S/N \sim 2$). In the case of a standard deviation of 1.8 ($S/N \sim 4$), the long-term trend was well reproduced. Hence, our model is validated if polarization flares are detected with $S/N \gtrsim 3$ in the case of Data (a). In general, the allowable S/N highly depends on the data itself. It is possible that a higher S/N is required for data with a higher flare-frequency.

Data (d) shows more complicated temporal variations. It was generated with a high flare frequency of $\alpha = 0.30$, and a more prominent long-term trend. Almost no characteristic of the long-term trend is seen in the middle panel of Data (c) in figure 2, and the path in the QU plane is apparently erratic as generally observed in blazars. Nevertheless, the long-term trend was successfully reproduced by the Bayesian model, as seen in the right panel of figure 2. While there is no significant correlation between the observed PF and the light curve, the correlation coefficient between PF_S and the light curve is calculated to be $0.84^{+0.05}_{-0.07}$. This demonstrates that the Bayesian method can be a powerful tool for the analysis of apparently erratic variations in polarization. We note that residuals between PF_S and the light curve are larger than those in the case of Data (a) and (b). This indicates that the Bayesian model possibly fails to reproduce the long-term trend in the case of a very high flare frequency.

In Data (e), there is no association between the light curve and the polarization parameters. The light curve was generated in the same way as in the other cases with $\alpha = 0.30$. The variation of the polarization vector was set to be a purely random walk in the QU plane without a long-term trend. The Bayesian model found a solution of the long-term trend even in this case, as shown in the right panel of Data (d) in figure 2. On the other hand, there is no significant correlation between the estimated PF_S and the light curve. This suggests that the model cannot extract any meaningful long-term trend from Data (d).

2.3. Evaluation of the Result Obtained from the Bayesian Model

In the last section, we demonstrated that the Bayesian model successfully reproduced the assumed long-term trends in the QU plane for the artificial data. It can, however, generate a false long-term trend even from the data in which no long-term trend was actually present. This is problematic for the application of this model to real observations in which we have no information about the presence of the long-term trend. Hence, we need to make a criterion for the validation of obtained results from the Bayesian model. We also need to determine the preferable range of the hyperparameter, w , because the result depends on w . In general, a hyperparameter in an empirical Bayesian model can be estimated by maximizing

marginal likelihood. This standard method is, however, insufficient in our model, as discussed in subsection 4.1. Here, we make a specific criterion for our model.

First, the correlation of PF_S and the light curve should be significantly improved compared with that of the observed PF and the light curve. The significance of the difference in two correlation coefficients is evaluated by Z -test. Using two correlation coefficients, r_i ($i = 1$ or 2), the test statistic, Z , which has a standard normal distribution, is defined as follows:

$$Z = (Z_1 - Z_2)/\sigma, \quad (8)$$

$$Z_i = \frac{1}{2} \log \left(\frac{1 + r_i}{1 - r_i} \right), \quad (9)$$

$$\sigma = \sqrt{\sigma_{Z_1}^2 + \sigma_{Z_2}^2}, \quad (10)$$

$$\sigma_{Z_i} = \frac{1}{\sqrt{N_i - 3}}, \quad (11)$$

where N_i is the number of samples. We can conclude that the two correlation coefficients are significantly different with a > 95 % confidence level when $|Z| > 1.96$. In our Bayesian model, a smaller w yields a smoother long-term trend, and hence results in a less improvement in the correlation coefficients between PF_S and the light curve. As a result, a too small w is discarded by this procedure. $|Z|$ were calculated to be 23.74, 17.41, 9.71, 6.86, and 1.35 in the case of the artificial data (a), (b), (c), (d), and (e) in the last subsection, respectively. Thus, we conclude that the long-term trend estimated for Data (e) is a false result.

Second, we need to check whether an estimated long-term trend actually has a longer time-scale than short-term variations. As mentioned in subsection 2.1, a long-term component is expected to depict a smooth path in the QU plane, and adopted the prior distribution with w . In other words, the hyperparameter, w , is related to the variation time-scale of the long-term trend in our model. A path of the long-term trend becomes more complicated and erratic in the case of a larger w (for example, see figure 5 in subsection 3.2). With an extremely large w , the variation amplitudes and time-scales of Q_L and U_L can be comparable to those of Q_S and U_S . Thus, w should be restricted to be small enough to assure that the estimated Q_L and U_L actually exhibit “long”-term variations. We evaluate it using a travel distance in the QU plane of both long- and short-term components. The travel distance, d , is defined for a set of $\{Q_i, U_i\}$ as follows:

$$d = \sum_{i=1}^{N-1} \sqrt{(Q_{i+1} - Q_i)^2 + (U_{i+1} - U_i)^2}. \quad (12)$$

In this paper, the estimated Q_L and U_L are acceptable in the case that the ratio of d for long- and short-term components, d_L and d_S , satisfies the following condition:

$$R = \frac{d_L}{d_S} < 0.10. \quad (13)$$

We call R as the “distance ratio”. In conjunction with the first criterion about the correlation coefficient, we can restrict w in a narrow range.

Results obtained by the Bayesian model are quantitatively evaluated by the above criterion. It is, however, possible that a false long-term trend would be extracted from observations even the result satisfies the above criterion. Hence, results from the Bayesian model should be evaluated carefully. In addition to the above criterion, we can check the validity of results with their qualitative features. We expect that a long-term trend exhibits not a random walk, but a systematic motion in the QU plane. A long-term trend depicting a very complicated path in the QU plane may merely indicate that there is no systematic long-term trend in the observed QU . We should also suspect a result highly sensitive to a small change in w .

3. Results: Application for Observed Photopolarimetric Data of Blazars

3.1. Data Description

We applied the Bayesian model to observed polarimetric data of blazars. The data were obtained with TRISPEC attached to the “Kanata” 1.5-m telescope at Higashi-Hiroshima Observatory during our photopolarimetric observation campaign for blazars in 2008–2009 (Watanabe et al. 2005; Uemura et al. 2008). A full description about the observation and the data reduction will be published in a forthcoming paper. In this paper, we focus on how our model works in the real data.

We used the V -band photopolarimetric data of OJ 287, S5 0716+714, and S2 0109+224. The observations of these three objects were performed in 79 nights between Oct 2008 and May 2009, 118 nights between Aug 2008 and May 2009, and 56 nights between Jul 2008 and Feb 2009, respectively. The light curves, PD, PF, and PA are shown in panels (a), (b), (c), and (d) in figure 4, respectively. Variations in the QU plane are shown in figure 5.

OJ 287 exhibited short-term flares having a time-scale of days superimposed on a gradual fading trend in the light curve. In contrast, PD remained high with 10–20% during the observation period, occasionally showing flares reaching maxima of $\sim 30\%$. The object almost stayed in the fourth quadrant in the QU plane. This behavior implies the presence of two polarization components, that is, one for a long-term trend pointing to the fourth quadrant, and the other for short-term flares.

Short-term variations in S5 0716+714 had features similar to that in OJ 287, while the behavior of PD is totally different. The PD of S5 0716+714 rapidly fluctuated between 0 and 15%. No systematic variation correlating with the total flux can be seen in the PD variation, except for a possible anti-correlation during a flare around MJD 54750. The temporal variation in the QU plane is very erratic.

S2 0109+224 experienced a flare clearly associated with an increase of PD around MJD 54810–54820. Except for this flare, no clear correlation can be seen between the light curve and PD. The PA apparently shows a systematic long-term trend; a gradual decreasing trend until MJD 54800, followed by an increasing trend, while short-

Table 1. Test statistics, $|Z|$, and Distance ratio, R , in the case of OJ 287, S5 0716+714, and S2 0109+224.

	OJ 287	S5 0716+714	S2 0109+224
w/σ	$ Z , R$		
0.10	1.08, 0.04	0.33, 0.03	1.66, 0.04
0.20	2.85, 0.09	0.40, 0.06	2.27, 0.07
0.30	3.97, 0.14	1.39, 0.09	2.26, 0.10
0.40	4.66, 0.18	2.25, 0.13	2.75, 0.11
0.50	4.78, 0.21	2.38, 0.15	2.83, 0.16

term variations occasionally disturb the trend. This behavior in PA indicates the presence of long- and short-term polarization components, as in OJ 287.

3.2. Bayesian Analysis of the Polarization Data

The Bayesian estimation of the long-term trend was performed for these three objects with $w/\sigma = 0.10, 0.20, 0.30, 0.40,$ and 0.50 . The different w/σ were used in order to check the dependency of results on w . Figure 5 shows the estimated long-term trends in the QU plane indicated by the filled circles. The top, middle, and bottom panels show the results with $w/\sigma = 0.10, 0.20,$ and $0.50,$ respectively. The long-term trends draw more complicated paths in the QU plane with larger w/σ , as expected. The test statistics, $|Z|$, and distance ratio, R , defined in subsection 2.3 for those results are summarized in table 1. Only the cases of $w/\sigma = 0.20$ for OJ 287 and S2 0109+224 are acceptable in our criterion; $|Z| > 1.96$ and $R < 0.10$. Temporal variations of PF and PA of the short-term components are shown in panels (e) and (f) of figure 4, respectively. Those of the long-term trends are in panels (g) and (h). Those panels show the results with $w/\sigma = 0.20$.

The long-term trend in S5 0716+714 draws a rather erratic path in the QU plane even with $w/\sigma = 0.10$. The two-component model is probably inadequate to explain the observed QU variation in S5 0716+714. The QU variation in S5 0716+714 may be caused by a number of polarization components having a variation time-scale of < 1 d (Moore et al. 1982; Jones et al. 1985). In this case, the time resolution of our observation could be too low to detect systematic variations of polarization. Rapid variations having a time-scale of less than hours have been actually reported in S5 0716+714 (Stalin et al. 2006; Sasada et al. 2008).

As can be seen from figure 4 and 5, the PA of the long-term trend in OJ 287 gradually increases until MJD 54920, and then decreases with time. In other words, the polarization vector apparently oscillates between a narrow range of PA of 150° – 170° smoothly in the observation period. This feature of the long-term trend can be seen both in the case of $w/\sigma = 0.10$ and 0.20 , which indicates that it is a stable feature. The PF of the long-term trend shows variations with a small amplitude of a factor ~ 2 . The long-term trend estimated in OJ 287 would, thus, be an ideal example for our two-component model.

In the case of S2 0109+224, the PF of the long-term

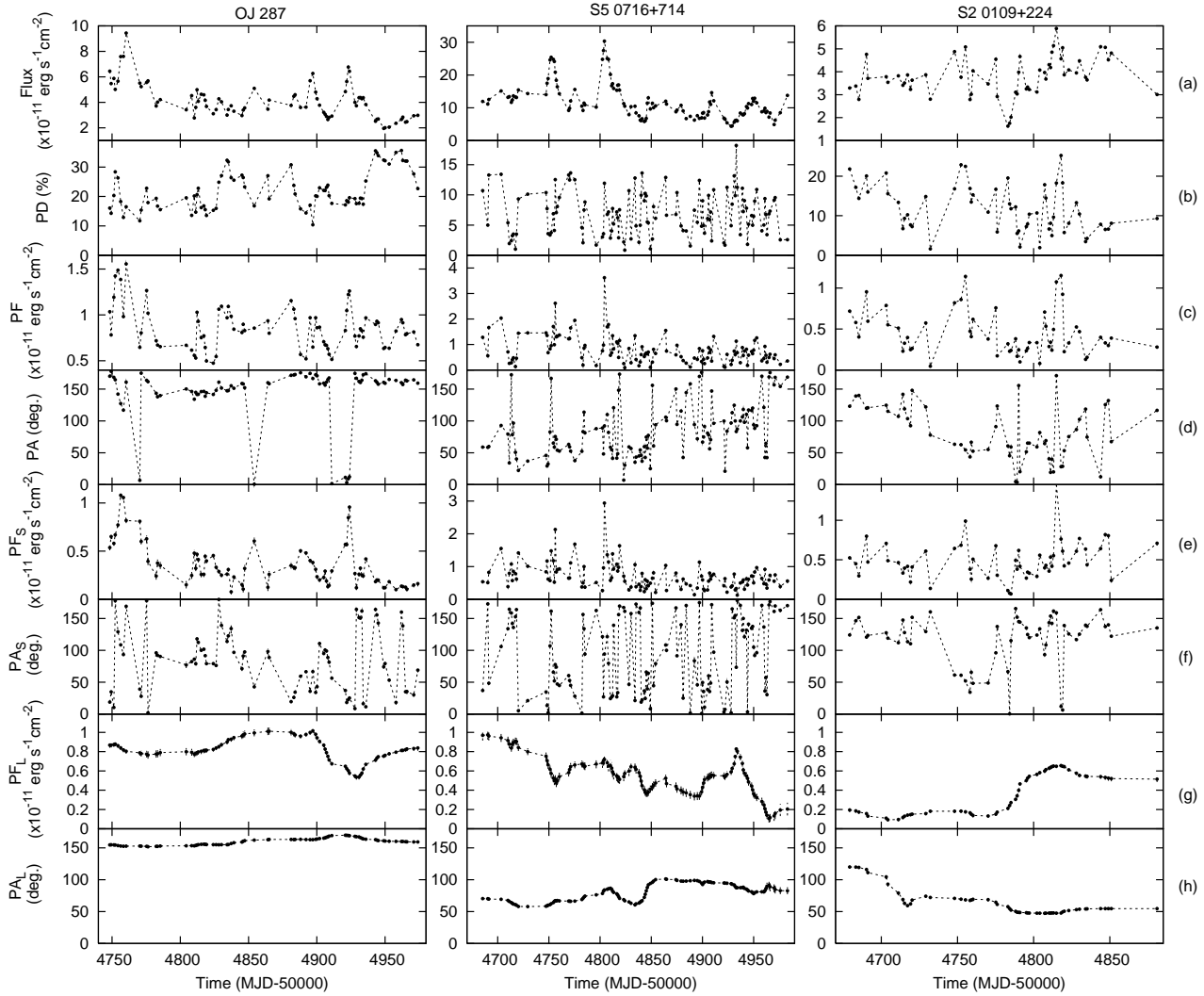


Fig. 4. Temporal variations of the observed and estimated parameters. The left, middle, and right panels show the results of OJ 287, S5 0716+714, and S2 0109+224, respectively, as indicated at the top of the panels. From top to bottom, the panels show (a) the observed light curve, (b) the observed polarization degree, (c) the observed polarized flux, (d) the observed polarization angle, (e) the estimated polarization flux of the short-term component, (f) the estimated polarization angle of the short-term component, (g) the estimated polarization flux of the long-term component, and (h) the estimated polarization angle of the long-term component. The observation errors and 1- σ confidence level of the estimated parameters are also indicated, while most of them are comparable with the symbol size.

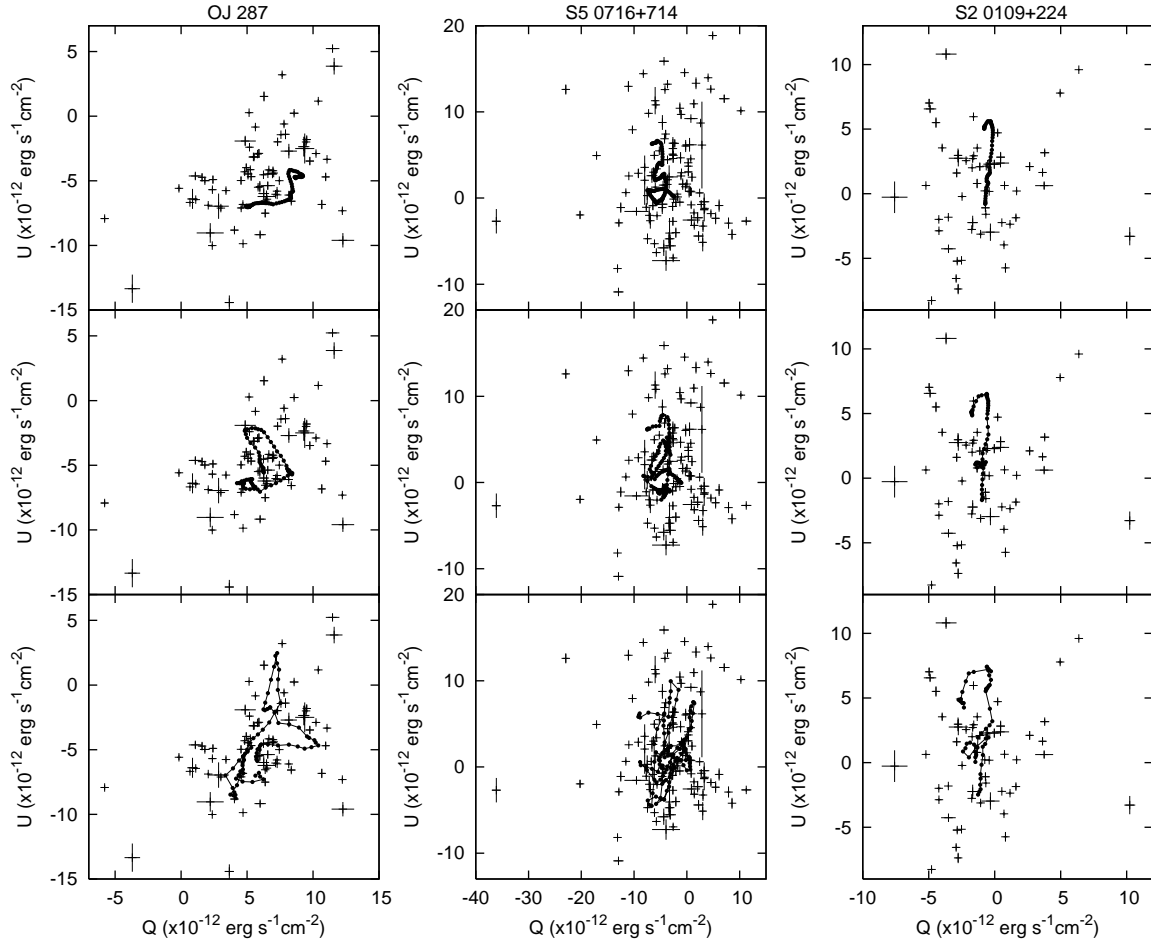


Fig. 5. Observed QU variations and estimated long-term trends. The left, middle, and right panels show the data of OJ 287, S5 0716+714, and S2 0109+224, respectively, as indicated at the top of the panels. The long-term trends were estimated with $w/\sigma = 0.10, 0.20,$ and 0.50 in the top, middle, and bottom panels, respectively. The observations and errors were indicated by the crosses. The long-term trends were indicated by the filled circles. The errors for each point of the estimated long-term trends are typically less than $0.3, 1.5,$ and $0.3 \times 10^{-12} \text{ erg s}^{-1} \text{ cm}^{-2}$ for OJ 287, S5 0716+714, and S2 0109+224, respectively.

trend first decreased until \sim MJD 54710, and then, the object stagnated near the origin of the QU plane for 40 d. After that, the PF increased with the opposite direction to the early trend in the QU plane, as shown in figure 5. This component turned to decrease again at last. This feature can be commonly seen in all cases of w/σ , while substructures become prominent in the case of $w/\sigma = 0.50$. This behavior of the long-term trend may be interpreted as two distinct components; one which kept decaying until \sim MJD 54710, and the other which became prominent later. We note that the PF of the long-term trend shows a large variation with a factor of ~ 7 . Since our two-component model assumes no flux variation for the long-term trend, the large variation amplitude of PF might violate this assumption. The problem can be reconciled only when the long-term trend exhibits a major variation in PD with a constant total flux.

The most notable feature in the estimated short-term component is nonuniform distributions in PA in S2 0109+224 and possibly also OJ 287. Figure 6 shows

the histograms of the PA of the short-term components. The figure also includes the distribution in S5 0716+714 just as a reference. We tested the nonuniformity of the distributions using the Kolmogorov-Smirnov (KS) test. As a result, KS probabilities were calculated to be 0.09, 0.05, and < 0.01 in the case of OJ 287, S5 0716+714, and S2 0109+224, respectively. Therefore, we confirmed that the nonuniformity is statistically significant in S2 0109+224 with a $> 95\%$ confidence level (, or KS probability < 0.05). This indicates that the PA of the short-term component is not completely random, and hence implies that the source of the short-term variation preferentially localizes in an area where the direction of the magnetic field is possibly fixed.

Finally, we note that small w were actually rejected in all cases of the three objects because no significant improvement was achieved in the correlation between the total and polarized flux, as shown in table 1. This means that too simple long-term trends are insufficient for our model. The most simple long-term component would be

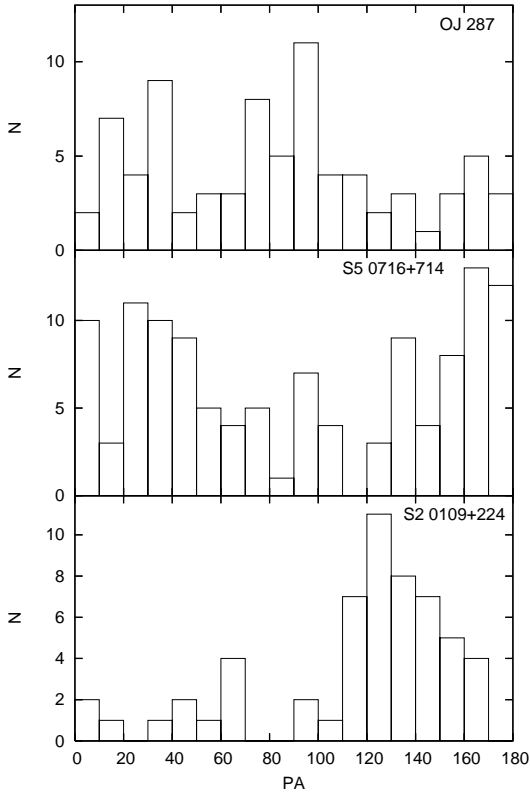


Fig. 6. Histogram of PA of the short-term component obtained with $w/\sigma = 0.20$. The top, middle, and bottom panels show the histograms for OJ 287, S5 0716+714, and S2 0109+224, respectively.

considered as averages of Q and U during the observation period. If the correlation would be improved with the differential polarization flux from the average (Q, U) , the Bayesian model was not required. However, we confirmed that the correlation is not significantly improved with those differential polarization flux from the averages; $|Z| = 1.22, 0.40, \text{ and } 1.27$ for OJ 287, S5 0716+714, and S2 0109+224, respectively. Our Bayesian model, therefore, has an advantage to extract long-term trends from polarization variations, compared with the simple correction with the average (Q, U) .

4. Discussion

4.1. Estimation of the Hyperparameter, w , by Maximizing Marginal Likelihood

As mentioned in subsection 2.3, we made the criterion to determine an appropriate value of the hyperparameter, w , in our Bayesian model. In general, a hyperparameter of an empirical Bayesian model can be estimated by maximizing a marginal likelihood. The marginal likelihood, M , is equivalent with the constant, C , in equation (2), defined as:

$$M(w) = \frac{L(\mathbf{y}|\mathbf{x})\pi(\mathbf{x}|w)}{P(\mathbf{y}|\mathbf{x})}. \quad (14)$$

Table 2. Marginal likelihood, $M(w)$, calculated with different w/σ .

w/σ	OJ 287	S5 0716+714	S2 0109+224
		$\times 10^3$	
0.10	2.06	2.86	0.97
0.50	2.96	3.96	1.92
1.00	3.20	4.44	2.16
2.00	3.21	4.61	2.21
3.00	2.99	4.53	2.22
5.00	2.60	4.15	2.17

We calculated $M(w)$ based on the method described in Chib & Jellazkov (2001). The model parameter, \mathbf{y} , can be arbitrary since $M(w)$ is independent of \mathbf{y} . The numerator of equation (14) was calculated with the estimated best parameters of \mathbf{y} . The denominator can be estimated by the Monte Carlo integration drawing a sample from $P(\mathbf{y}|\mathbf{x})$ which were obtained by our Bayesian analysis. The results are summarized in table 2.

$M(w)$ takes the maximum with $w/\sigma = 2.00\text{--}3.00$ for all cases of the three objects. A long-term component estimated with such a large w/σ definitely draws a quite complicated path in the QU plane, as can be seen from figure 5. As a result, it is not acceptable in our criterion about the distance ratio, R .

The ratio of two $M(w)$ is called the ‘‘Bayes factor’’ (BF), which used to evaluate the models. The BF are calculated to be $\sim 1.6, \sim 1.6, \text{ and } \sim 2.3$ with $M(0.10)$ and the maximum of M for OJ 287, S5 0716+714, and S2 0109+224, respectively. These BF are too small to conclude that the model with $w/\sigma = 2.00\text{--}3.00$ is significantly better than that with $w/\sigma = 0.10$ (Kass & Raftery 1995).

Thus, the maximization of $M(w)$ is not suitable to determine w in our model. This is mainly because the prior distribution is not the real distribution for Q_L and U_L . Another form of the prior distribution may be more suitable for the case of polarization variations in blazars. The practical criterion defined in subsection 2.3 is enough for our exploratory model in this paper.

4.2. Application in the $(Q/I, U/I)$ Plane

Our Bayesian model can find a long-term trend in the QU plane. It can be also applied in the $(q, u) = (Q/I, U/I)$ plane, while strong limitations are imposed for the application. In our two-component model, the observed (q, u) is described as:

$$q = \frac{Q_L + Q_S}{I_{\text{total}}}, u = \frac{U_L + U_S}{I_{\text{total}}} \quad (15)$$

$$I_{\text{total}} = I_L + I_S. \quad (16)$$

The two polarization components, namely, $(q_L, u_L) = (Q_L/I_L, U_L/I_L)$ and $(q_S, u_S) = (Q_S/I_S, U_S/I_S)$, can be separated in the qu plane when q_L and u_L are much smaller than q_S and u_S (e.g. Messenger et al. 1997). If the PD of the long-term trend is not negligible, the polarization components cannot be separated without the estimation of I_L and I_S .

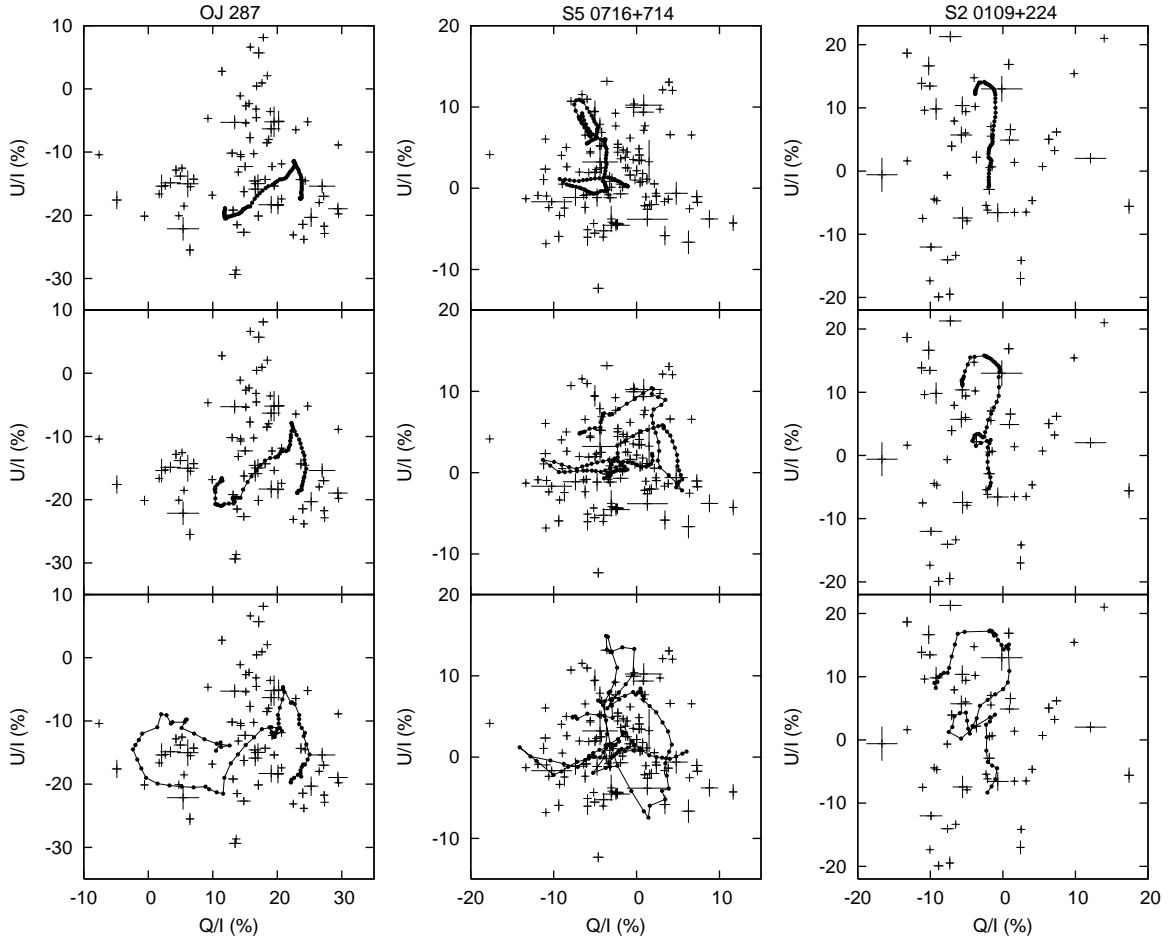


Fig. 7. Same as figure 5, but for Q/I and U/I . The errors for each points of the estimated long-term trends are typically less than 1.0, 1.3, and 0.9 % for OJ 287, S5 0716+714, and S2 0109+224, respectively.

In the case that the PD of the long-term trend is large, the application of the Bayesian model in the qu plane means the estimate of $(Q_L/I_{\text{total}}, U_L/I_{\text{total}})$ that lead to a positive correlation between the light curve and the modified PD calculated from $(Q_S/I_{\text{total}}, U_S/I_{\text{total}})$. Since I_L is assumed to be time-independent in our model, the temporal behavior of the estimated $(Q_S/I_{\text{total}}, U_S/I_{\text{total}})$ is probably analogous to that of $(Q_S/I_S, U_S/I_S)$. In this sense, the Bayesian analysis in the qu plane is not completely nonsense, and can still provide meaningful results. A result in the qu plane would be noteworthy, particularly if the long-term trend in the qu plane draws an analogous path to that in the QU plane.

Figure 7 is the same as figure 5, but for the qu plane. We found that the long-term trends estimated with $w/\sigma = 0.20$ are quite analogous to those in figure 5 in the case of S2 0109+224. The long-term trend in OJ 287 also exhibits a common feature with that in the QU plane in terms of the oscillation of the polarization vector within a narrow range of PA. The similarity between the long-term trends in the QU and qu planes implies that the short-term flares were associated with the increases of PD in OJ 287 and

S2 0109+224. The short-term flares may originate from a region where the direction of the magnetic field is more aligned than the whole emitting region.

4.3. Future Studies

We showed that the polarization vector in OJ 287 and S2 0109+224 can be separated into two components, the long-term trend and the short-term variation component. The result, however, provides no clear evidence for the existence of the two components in these objects. Our Bayesian model just gives us one of possible views for temporal variations of polarization in blazars. This view deserves to be discussed since simple and systematic variations can be extracted from apparently erratic variations. On the other hand, further investigations are needed to confirm the two-component view.

One of the most direct ways to obtain evidence for the two-component scenario would be VLBI radio observations. Marscher et al. (2002) reported the presence of multiple polarization components even within radio cores in blazars. VSOP-2 is a space VLBI project, which will resolve sub-pc regions around the central blackhole of AGN (Hirabayashi et al. 2004). VSOP-2 will reveal the detailed

structure of the polarization components in the radio core. A part of the radio polarization components might exhibit temporal variations synchronized with the optical polarization components resolved by our Bayesian model. If this is the case, our Bayesian model, for the first time, provides a tool to investigate the temporal evolution of each polarization component observed both in the optical and radio regimes.

Our model assumes that the PF of the short-term component correlates with the light curve of the total flux (condition “ii”) in section 2.1). In other words, we assume the total flux exhibits a flare whenever a short-term polarization flare occurs. This assumption gives the condition that the application of our Bayesian model is validated. Our model definitely yields a false result if it applies to, for example, short-term polarization flares without significant variations of the total flux. If such variations are typical in a blazar, our model is not validated for it. Our assumption should, hence, be evaluated case by case for objects. In our picture, a short-term flare with a larger amplitude is expected to show a better correlation with polarization because the specific polarization-feature of a smaller flare would be readily diluted by another small flares. Hence, the polarization behavior of short and large flares would provide a key for the validation of our assumption.

Marscher et al. (2008) reported a rotation of the optical polarization vector in BL Lac and interpreted it as a shift of the emitting region through a helical magnetic field in the jet. Such a rotation event can have been missed if the observed polarization has a long-term trend as considered in our model. Our Bayesian model would provide a tool to search the rotation events of the polarization vector both in the observed, long- and short-term components. No systematic rotation event can be seen in the long- and short-term components in the three objects, as shown in subsection 3.2.

5. Summary

We developed a Bayesian model to extract a long-term trend from apparently erratic variations in polarization of blazars. Our Bayesian model successfully resolved the long- and short-term components in the artificial data. We applied this model to the photopolarimetric data of OJ 287, S5 0716+716, and S2 0109+224. Simple and systematic long-term trends were obtained in OJ 287 and S2 0109+224, while no meaningful trend was identified in S5 0716+716. We propose that all short-term flares were associated with the increase of the polarized flux in OJ 287 and S2 0109+224. The polarization variation in S5 0716+716 may be explained by a random variation caused by a number of polarization components having a quite short time-scale of variations.

We acknowledge useful discussions with Taichi Kato and Takuya Yamashita. This work was partly supported by a Grand-in-Aid from the Ministry of Education, Culture, Sports, Science, and Technology of Japan (19740104).

References

- Angel, J. R. P. & Stockman, H. S. 1980, *ARA&A*, 18, 321
 Blandford, R. D. & Rees, M. J. 1978, in *BL Lac Objects*, ed. A. M. Wolfe (Pittsburgh: University of Pittsburgh Press), 328
 Blinov, D. A. & Hagen-Thorn, V. A. 2009, *A&A*, 503, 103
 Cellone, S. A., Romero, G. E., Combi, J. A., & Martí, J. 2007, *MNRAS*, 381, L60
 Chib, S. & Jellazkov, I. 2001, *Journal of the American Statistical Association*, 96, 270
 Efimov, Y. S. & Shakhovskoy, N. M. 1998, *BLAZAR Data*, 1, 3
 Hagen-Thorn, V. A., Larionova, E. G., Jorstad, S. G., Björnsson, C.-I., & Larionov, V. M. 2002, *A&A*, 385, 55
 Hirabayashi, H., Murata, Y., Asaki, Y., Edwards, P. G., Mochizuki, N., Natori, M. C., Inoue, M., Umemoto, T., et al. 2004, *Proc. SPIE*, 5487, 1646
 Hufnagel, B. R. & Bregman, J. N. 1992, *ApJ*, 386, 473
 Impey, C. D., Malkan, M. A., & Tapia, S. 1989, *ApJ*, 347, 96
 Jones, T. W., Rudnick, L., Fiedler, R. L., Aller, H. D., Aller, M. F., & Hodge, P. E. 1985, *ApJ*, 290, 627
 Kass, R. E. & Raftery, A. E. 1995, *Journal of the American Statistical Association*, 90, 773
 Kataoka, J., Takahashi, T., Wagner, S. J., Iyomoto, N., Edwards, P. G., Hayashida, K., Inoue, S., Madejski, G. M., et al. 2001, *ApJ*, 560, 659
 Marscher, A. P., Jorstad, S. G., D’Arcangelo, F. D., Smith, P. S., Williams, G. G., Larionov, V. M., Oh, H., Olmstead, A. R., et al. 2008, *Nature*, 452, 966
 Marscher, A. P., Jorstad, S. G., Mattox, J. R., & Wehrle, A. E. 2002, *ApJ*, 577, 85
 Mead, A. R. G., Ballard, K. R., Brand, P. W. J. L., Hough, J. H., Brindle, C., & Bailey, J. A. 1990, *A&AS*, 83, 183
 Messinger, D. W., Whittet, D. C. B., & Roberge, W. G. 1997, *ApJ*, 487, 314
 Metropolis, N. 1953, *The journal of chemical physics*, 21, 1087
 Moore, R. L., Angel, J. R. P., Duerr, R., Lebofsky, M. J., Wisniewski, W. Z., Rieke, G. H., Axon, D. J., Bailey, J., Hough, J. M., & McGraw, J. T. 1982, *ApJ*, 260, 415
 Sasada, M., Uemura, M., Arai, A., Fukazawa, Y., Kawabata, K. S., Ohsugi, T., Yamashita, T., Isogai, M., Sato, S., & Kino, M. 2008, *PASJ*, 60, L37
 Smith, P. S., Balonek, T. J., Heckert, P. A., & Elston, R. 1986, *ApJ*, 305, 484
 Stalin, C. S., Gopal-Krishna, Sagar, R., Wiita, P. J., Mohan, V., & Pandey, A. K. 2006, *MNRAS*, 366, 1337
 Takahashi, T., Kataoka, J., Madejski, G., Mattox, J., Urry, C. M., Wagner, S., Aharonian, F., Catanese, M., et al. 2000, *ApJL*, 542, L105
 Tosti, G., Fiorucci, M., Luciani, M., Efimov, Y. S., Shakhovskoy, N. M., Valtaoja, E., Teraesranta, H., Sillanpaae, A., et al. 1998, *A&A*, 339, 41
 Uemura, M., Sasada, M., Arai, A., Fukazawa, Y., Kawabata, K. S., Phsugi, T., Yamashita, T., Isogai, M., et al. 2008, in *Blazar Variability across the Electromagnetic Spectrum* (Proceedings of Science: SISSA)
 Watanabe, M., Nakaya, H., Yamamuro, T., Zenno, T., Ishii, M., Okada, M., Yamazaki, A., Yamanaka, Y., et al. 2005, *PASP*, 117, 870